

Article

Numerical Simulation of Extreme Ice Loads on Complex Pile Legs of Offshore Substation Structures

Baofeng Zhang^{1,2,3}, Rui Dong⁴, Wei Li^{1,3}, Yue Zhao^{1,3}, Guojun Wang⁴ and Dayong Zhang^{4,*}

¹ Key Laboratory of Far-Shore Wind Power Technology of Zhejiang Province, Hangzhou 311122, China; zhang_bf2@hdec.com (B.Z.); li_w@hdec.com (W.L.); zhao_y7@hdec.com (Y.Z.)

² College of Civil Engineering and Architecture, Zhejiang University, Hangzhou 310058, China

³ PowerChina Huadong Engineering Corporation Limited, Hangzhou 311122, China

⁴ School of Chemical Engineering, Ocean and Life Sciences, Dalian University of Technology, Panjin 124221, China; dongrui007@mail.dlut.edu.cn (R.D.); wgj@dlut.edu.cn (G.W.)

* Correspondence: zhangdy@dlut.edu.cn

Abstract: The sea ice failure mode and ice force amplitude depend on the structural form at the point of interaction, but the impacts of ice load when interacting with marine engineering structures with additional attachments are not yet clear. This study conducts numerical simulations using the discrete element method to investigate the interaction between sea ice and cable pipes attached to offshore substation structures. Various operating conditions such as ice velocity, ice thickness, and ice attack angle are selected to simulate the interaction between sea ice and such structures, clarifying the variations in the sea ice failure mode and ice force amplitude. The results indicate that crushing failure mainly occurs when sea ice interacts with such structures, and the presence of cable pipes does not alter the sea ice failure mode at the legs of offshore substation structures. The preliminary action of sea ice with cable pipes effectively reduces the ice load on the structure, and the minimum ice force amplitude occurs at an ice attack angle of 90°, with the ice force amplitude increasing with the ice thickness but showing no clear correlation with the ice velocity. The findings of this study provide a reference for the ice-resistant design of offshore substation structures in cold regions.

Keywords: cable pipe; sea ice failure mode; ice force amplitude; numerical simulation



Citation: Zhang, B.; Dong, R.; Li, W.; Zhao, Y.; Wang, G.; Zhang, D. Numerical Simulation of Extreme Ice Loads on Complex Pile Legs of Offshore Substation Structures. *J. Mar. Sci. Eng.* **2024**, *12*, 838. <https://doi.org/10.3390/jmse12050838>

Academic Editors: José António Correia and Eva Loukogeorgaki

Received: 1 April 2024
Revised: 10 May 2024
Accepted: 14 May 2024
Published: 17 May 2024



Copyright: © 2024 by the authors. Licensee MDPI, Basel, Switzerland. This article is an open access article distributed under the terms and conditions of the Creative Commons Attribution (CC BY) license (<https://creativecommons.org/licenses/by/4.0/>).

1. Introduction

Offshore wind power, widely acknowledged as a clean and renewable energy source, has garnered significant attention and emerged as a central focus in the ongoing evolution of global wind power [1]. In recent years, offshore wind energy resources have been greatly developed, and there have been significant advances in the design, construction, and installation technologies of large and super-large offshore wind power structures. For the construction, installation, and maintenance of offshore wind farms, extreme marine environmental conditions must be considered. Not only do offshore platforms need to withstand the weight of their own structures and equipment and operational dynamic loads, but they also need to cope with the effects and influences of wind, waves, currents, ice, vessels, drifting objects, and even earthquakes, among various variable loads. The action of cyclic loads is more likely to lead to decreased carrying capacity and fatigue damage. According to on-site monitoring results, the impact of ice loads on structures far exceeds that of other environmental loads. The study of the interaction between sea ice and structures plays a dominant role in structural design [2]. The Yellow and Bohai Seas, notable for their high latitudes and abundant wind energy density, stand out as pivotal areas for the progression of offshore wind power initiatives. In these regions, extensive efforts have been undertaken for the large-scale construction and development of offshore wind farms. During the winter season, the presence of sea ice presents a significant challenge to the development of offshore wind power. This poses a substantial threat to

the structural integrity of offshore structures, subjecting them to considerable loads and potentially resulting in significant damage.

Offshore wind farms in ice-covered regions encounter various challenges attributed to the existence of sea ice. The significance of sea ice must be carefully evaluated in the planning and implementation of offshore wind energy projects. Following interactions between sea ice and offshore structures, the potential occurrence of various types of failure, such as crushing failure, buckling failure, bending failure, and splitting failure, is influenced by factors such as the ice velocity, width-to-thickness ratio, and ice characteristics [3]. The aforementioned destructive behaviors lead to structures that bear different levels of ice loads. Based on the various structural forms present at the interaction sites with sea ice, offshore structures in regions prone to ice can be classified into three categories: vertical structures, cone structures, and complex structures. Experts and scholars globally utilize various methods, including theoretical analyses, field measurements, numerical simulations, and model experiments, to investigate the properties of ice loads. In current offshore engineering structural design, auxiliary components are often added to enhance the safety and functionality of structures, such as collision prevention structures, berthing components, cable pipes, and ice-breaking structures. However, research on the interaction between sea ice and these structures is relatively limited. Therefore, it is necessary to conduct studies on the ice-resistant performance of offshore engineering structures with additional auxiliary components.

In terms of vertical structures, Timco et al. [4] examined ice load data collected from the Molikpaq platform, and observed that, in cases where sea ice undergoes crushing failure, the loads that it sustains significantly surpass the load thresholds observed during bending failure. Kärnä et al. [5,6] suggested that the interaction of ice with vertical structures predominantly leads to crushing and buckling failures. Different ice thicknesses and ice velocities affect the sea ice failure modes. Hendrikse et al. [7] indicated that, when flexible vertical structures are exposed to horizontal ice action, they primarily undergo crushing failure. Buckling failure occurs when the sea ice sheet is thin or when the structure width is significantly larger than the ice thickness. This results in ice failure when the stress caused by buckling surpasses the bending strength of the sea ice. Yue et al. [8] observed a strong correlation between loading speed and the failure modes of sea ice, as indicated by field monitoring data. With the acceleration of ice velocity, sea ice undergoes a transition from ductile failure to ductile–brittle transition failure and eventually to brittle failure. Sanderson [9] analyzed the sea ice failure mode of vertical structures in the field and found that sea ice usually undergoes buckling failure when the ice sheet is thin and crushing failure when the ice sheet is thick. Ji et al. [10] studied the interaction between sea ice and offshore engineering structures based on the discrete element method, observed the sea ice failure process, and calculated the ice vibration response of the structure to provide data support for its fatigue life assessment. Long et al. [11] utilized the discrete element method to simulate the interaction between sea ice and offshore wind turbines, investigating the sea ice failure mode and structural vibrations at different ice velocities, as well as revealing the correlation between self-excited vibrations and the ductile–brittle transition of sea ice.

In terms of cone structures, Izumiyama et al. [12] found that, in interactions between sea ice and cone structures, radial cracks occur before circumferential fractures. Li [13] conducted an analysis of the interaction process between ice and the JZ20-2MUQ platform. The study revealed that narrow cones demonstrate wedge-shaped bending failure, and plate-shaped bending failure was also observed. Paavilainen et al. [14] employed the two-dimensional combined finite–discrete element method to model the interaction between sea ice and a wide sloping structure, and they found that, with thin ice, the effects of the ice–ice friction coefficient and ice compressive strength on ice load are minimal, while with thick ice, the impact of the friction coefficient on ice load increases only under low-compressive-strength conditions. Qu et al. [15] conducted a stochastic analysis of the ice load data measured on pressure boxes, revealing the statistical characteristics of ice force amplitude and frequency for cone structures. Ranta et al. [16–18] carried out a simulation

of the interaction process between ice and inclined structures utilizing the two-dimensional combined finite–discrete element method. Their findings indicate that peak ice loads are influenced by buckling. Di et al. [19] utilized the discrete element method to model the interaction dynamics among level ice, fragmented ice, and cone wind turbine structures. They revealed that level ice exerts higher ice loads on conical structures than fragmented ice. Jou et al. [20] employed the discrete element method to model the interaction dynamics among level ice, floating ice, and icebreaking vessels or icebreaking cones. They examined variations in ice damage features across various scenarios.

Offshore substation structures play a crucial role in connecting offshore wind turbines to the power grid. The technological advancement of these facilities significantly impacts the rate of development of offshore wind power [21]. A jacket structure is commonly utilized as the support system for offshore substation structures. To enable transmission functionality, cable pipes are typically positioned in close proximity to the pile legs. The presence of cable pipes is crucial when examining the interaction between sea ice and structures. For offshore engineering structures with additional auxiliary components, based on years of field measurements of the interaction between sea ice and jack-up platforms, Zhang et al. [22] investigated the interaction between sea ice and a jack-up platform with gear teeth through model tests. They found that, despite the interaction with the structure, sea ice still experienced crushing failure, and the presence of gear teeth did not fundamentally alter the ice failure mode. Due to the significant difference in size between the gear teeth and the legs of the jack-up platform, the impact on structural ice loads was relatively minor. Liu et al. [23] investigated the interaction between sea ice and the high-pile cap foundation of offshore wind power with a berthing component through model tests. They analyzed the ice loads on the structure under varying ice velocities and ice attack angles. Their findings revealed that the presence of the berthing component led to the accumulation of failure of the ice sheet, consequently reducing the ice force amplitude exerted on the structure. Because of the larger dimensions of the berthing component, sea ice not only experiences crushing failure but also undergoes bending failure. The enterprise standard Q/HSn 3000 of the China National Offshore Oil Corporation (CNOOC) specifies a method for calculating ice loads on arrays of conductors [24]. It introduced the concept of the shielding coefficient and provides reference standards for the ice force amplitude from different ice action directions. However, this calculation method is applicable only to group pile structures with a relatively small spacing.

Based on the above discussion, it can be observed that the research on the interaction between ice and regular vertical structures and conical structures is relatively mature, with researchers obtaining corresponding results through theoretical analyses, model experiments, and field monitoring. However, for offshore substation structures with additional cable pipes, the introduction of auxiliary components to smooth cylindrical pile legs makes the failure modes that occur on this structure due to ice action much more complex than those that occur on vertical and conical structures. Research has not been conducted on ice loads on such structures, and the extent to which cable pipes affect ice loads remains unknown; thus, this study takes this as the research content. The numerical simulation method is used to analyze the change rule of the ice load on the structure and the influence on the sea ice failure mode after adding cable pipes, and a comparison is made with the ice load on smooth cylindrical pile legs. Additionally, this study seeks to outline the impacts of ice load on complex structures and offer suggestions for the ice-resistant design of these structures.

2. Numerical Simulation of Interaction between Sea Ice and Offshore Substation Structures

2.1. Numerical Simulation Methods

The research on ice loads primarily utilizes four methodologies: on-site measurements, model tests, theoretical analyses, and numerical simulations. Based on model tests and on-site measurements, along with theoretical analyses, experts and scholars utilize numerical simulation methods to demonstrate the interaction process between sea ice and structures,

observing the dynamic ice-breaking process [25]. In studies of the interaction between ice and structures, the commonly used numerical analysis methods include the finite element method, the discrete element method, and the discontinuous deformation analysis method.

The finite element method can be used to simulate an intrinsic model of sea ice, as well as the fragmentation process in sea ice movement, and it can better deal with more complex mechanical models. Sea ice is a non-continuous medium and exhibits discrete characteristics after fragmentation. Although the finite element method can accurately describe the dynamic response of the structure, it cannot adequately simulate the brittle destruction of ice or the effects of the removal motion and interaction after fragmentation into small pieces of ice.

The discrete element method can be used to simulate the collision and friction between ice blocks at small scales, and it can also be used to numerically simulate the formation of ice ridges, the generation of ice leads, and the evolution process of large-scale polar sea ice at intermediate scales. Due to the discrete distribution mode of sea ice, the DEM can be used to better study the interaction between sea ice and offshore substation structures and to observe the change in the sea ice failure mode and ice load in the interaction process [26–28].

The discontinuous deformation analysis is a novel numerical analysis approach that combines mathematical topology with engineering practice. It can be used to simulate the interaction process between ice and structures, visualize the ice failure process, and calculate the structural dynamic response at each time step after ice impact, making the simulation of ice failure closer to reality. However, this method is relatively less used in ice load studies.

In this study, the discrete element method is utilized to investigate the correlations between sea ice failure modes and ice loads. This study observes different characteristics, such as the non-continuous distribution of ice block shapes and sizes, throughout the sea ice failure process [29]. The sea ice failure process during interactions with vertical structures is illustrated in Figure 1. In Figure 1b, it can be observed that the primary sea ice failure mode in the discrete element method simulation is crushing failure. After the interaction between the sea ice and the vertical structure, a significant amount of powder-like sea ice is generated, continuously squeezed out from the contact surface between the sea ice and the structure.

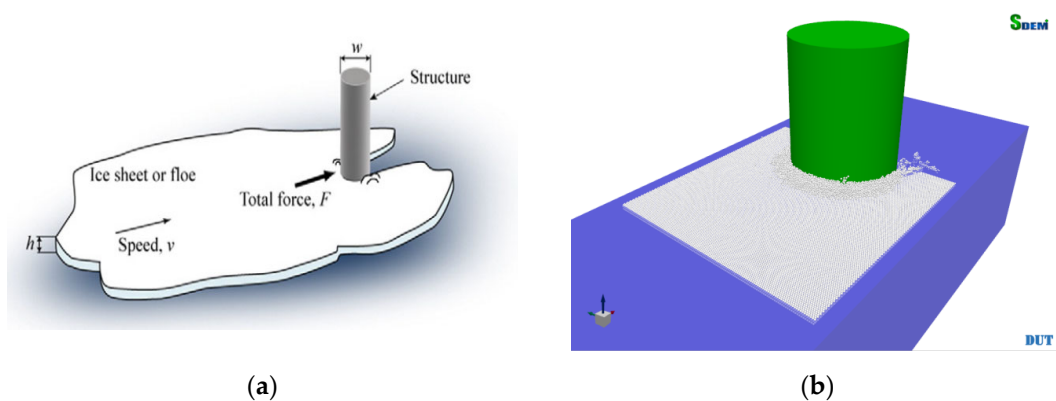


Figure 1. The interaction between sea ice and vertical structures: (a) schematic of sea ice interaction with vertical structures; (b) discrete element simulation of sea ice interaction with vertical structures.

2.2. Numerical Model

This study utilizes discrete element high-performance computing software (Software Patent No. CN104951601A) [30–32] to simulate the interaction between sea ice and structures, focusing on the ice failure modes and the calculation of ice loads on structures. The software employs viscoelastic and plastic models to describe the mechanical processes, such as crushing, bending, and buckling failure, between elements. The load model mainly consists of two parts: one simulates the fracture process between bonded sea ice elements, and the other simulates the frictional collision effects between non-frozen ice elements.

Sea ice is composed of spherical elements of uniform mass and size, arranged in a regular pattern, with the three non-contacting sides fixed using linear spring boundaries. Because of the effect of ice particle size, to maintain the same density of ice particles under different contact areas, the height of each layer of ice particles is kept consistent. The interaction between the ice particles uses an elastic–viscous contact model based on the Mohr–Coulomb theory [33], and a parallel bonding model is used when combining spherical ice particles into smooth ice. Two adjacent sea ice elements are considered bonded together through the parallel bonding model, with an elastic bonding disc set between the bonded particle units, as illustrated in Figure 2 [11]. Such a model can transmit both forces and moments, capable of withstanding certain tension and compressive forces, and they break upon collision with structures under the influence of ocean currents, thereby allowing for the study of sea ice failure modes [34,35].

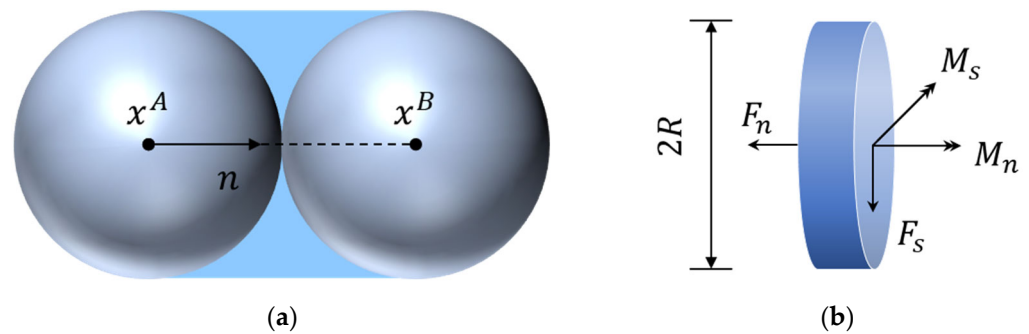


Figure 2. Parallel bond model for spherical elements: (a) schematic of bonding between sphere A and sphere B; (b) forces acting on the contact surface.

In the parallel bonding model, F_n and F_s represent the normal and tangential forces between particles, respectively, while M_n and M_s denote the normal and tangential moments between particles, respectively. The maximum tensile stress and maximum shear stress acting on the bonding disc can be expressed as follows:

$$\sigma_{max} = -\frac{F_n}{A} + \frac{|M_s|}{I}R \tag{1}$$

$$\tau_{max} = -\frac{F_s}{A} + \frac{|M_n|}{J}R \tag{2}$$

where R is the radius of the bonding disc; A is the area of the bonding disc; I and J are the moment of inertia and polar moment of inertia of the bonding disc, which can be calculated using the following equations:

$$A = \pi R^2, I = \frac{1}{4}\pi R^4, J = \frac{1}{2}\pi R^4 \tag{3}$$

When simulating the fracture process of sea ice, the failure mode of the bonding between units is categorized into crushing and shear failure based on the normal and tangential forces on the particle units. The bonding disc fails when the maximum tensile stress σ_{max} exceeds the tensile failure strength σ^t between the particle units, or when the maximum shear stress τ_{max} surpasses the shear failure strength τ^s between the particle units [11]. Figure 3 [30] illustrates the bonding failure model of particle units. The tensile failure strength σ^t and shear failure strength τ^s of the bonding units can be represented as follows:

$$\sigma^t = \sigma_b^n \tag{4}$$

$$\tau^s = \sigma_b^s + \mu_b \sigma_{max} \tag{5}$$

where σ_b^n and σ_b^s represent the normal and shear bonding strengths of the particle units, respectively, with $\sigma_b^n = \sigma_b^s$ assumed in this study; μ_b is the coefficient of internal friction, where $\mu_b = \tan \varphi$ and φ is the internal friction angle.

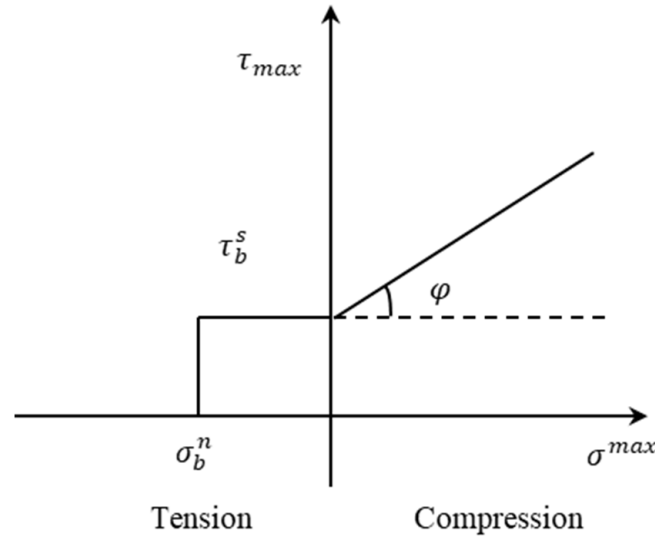


Figure 3. Bonding failure model of particle units.

To verify the accuracy of the discrete element method for sea ice and the selection of parameters, the numerical simulation results were compared with measured data from the JZ9-3 MDP-1 platform in Liaodong Bay, Bohai Sea, China. Ice conditions with a thickness of 0.2 m were simulated, and ice element diameters were set to 0.04 m, 0.05 m, 0.07 m, 0.1 m, and 0.2 m to compare the numerical simulation results with the on-site measured data. For an ice thickness of 0.2 m, the average ice force amplitude on the JZ9-3 MDP-1 platform was 66.78 kN. When the element diameter was set to 0.1 m, the numerical simulation results were closer to the on-site measured data, as shown in Figure 4.

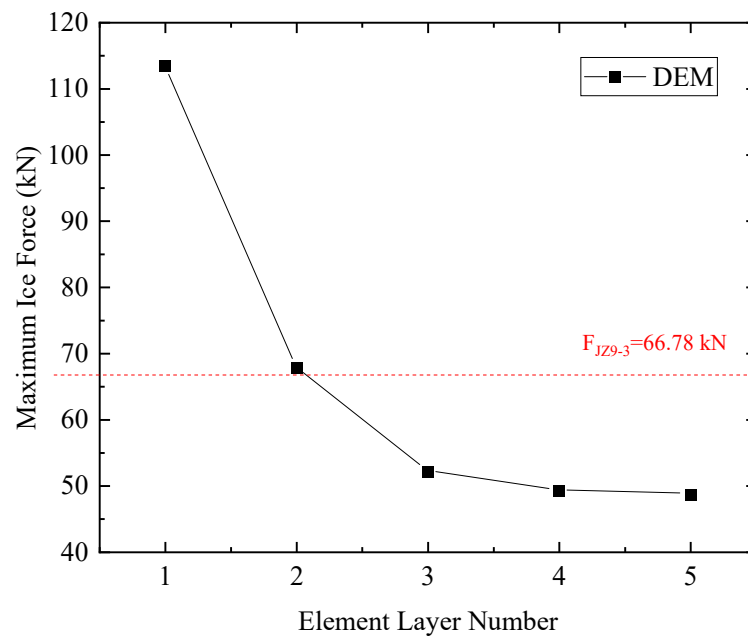


Figure 4. Comparison of numerical simulation results of average ice force under different particle sizes with field-measured data.

Numerical simulations were performed utilizing the dimensional parameters of a particular offshore substation structure. The essential structural parameters consisted of a pile leg diameter of 1.5 m with a wall thickness of 0.06 m, a cable pipe diameter of 0.508 m with a wall thickness of 0.02 m, and a center-to-center distance of 1.5 m between the two structural circles. The model structure is depicted in Figure 5, and the parameters for the calculations using discrete element software are outlined in Table 1.

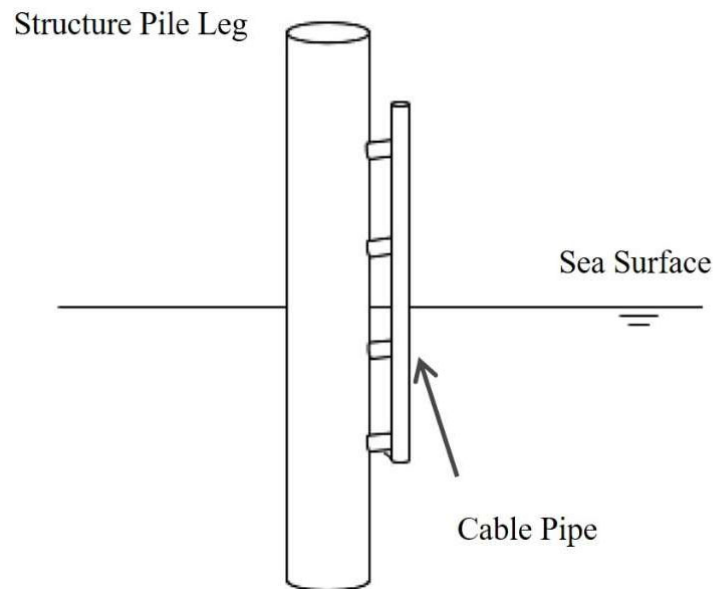


Figure 5. Schematic of sea ice interaction with offshore substation structure with a cable pipe.

Table 1. Key parameters for discrete element calculations.

Parameter	Symbol	Value	Parameter	Symbol	Value
Sea Ice Density/(kg/m ³)	p_{ice}	920.0	Element Diameter/m	d_1	0.1
Seawater Density/(kg/m ³)	p_w	1035.0	Distance Between Structure Centers/m	d_2	1.5
Sea Ice Elastic Modulus/GPa	E	1.0	Pile Leg Diameter/m	w_1	1.5
Sea Ice Compressive Strength/MPa	σ_c	2.0	Cable Pipe Diameter/m	w_2	0.508
Sea Ice Bending Strength/MPa	σ_f	0.7	Sea Ice Thickness/m	h	0.2/0.3/0.4
Sea Ice Friction Coefficient	u_{ice}	0.16	Sea Ice Velocity/(m/s)	v	0.01–0.1
Element Bonding Strength/MPa	σ_b	0.94	Ice Attack Angle/°	a	0–90

During the numerical simulation process, the dimensions chosen for the calculation domain of the level ice zone were 10 m × 7 m (length × width). Spring constraints were applied at the boundaries of the computational domain and between sea ice elements, with the stiffness of the springs set to be equal to the contact stiffness between the elements. Due to the presence of cable pipes, the support structure exhibits asymmetry. Therefore, simulations were conducted under different ice attack angles (defined as the angle between the ice normal and the structure centerline), including a 0° ice attack angle (vertical collision between the ice sheet and the side of the cable pipe and the support structure), 30° ice attack angle, 45° ice attack angle, 60° ice attack angle, and 90° ice attack angle (direct contact between the ice sheet and the front of the cable pipe). Additionally, scenarios without attached cable pipes were considered, resembling smooth cylinders. Ice thickness options were 0.2 m, 0.3 m, and 0.4 m (with an element diameter of 0.1 m), while ice velocities ranged from 0.01 to 0.1 m/s. The specific configurations are depicted in Figure 6.

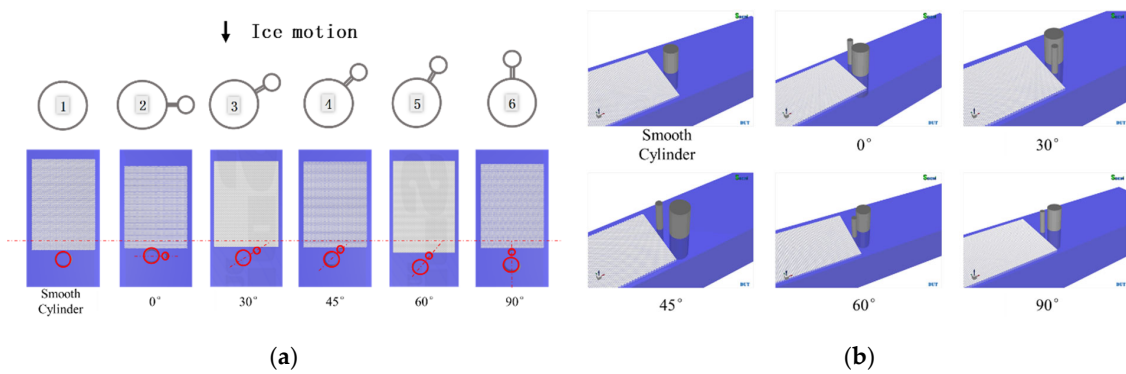


Figure 6. Simulation of interaction between structure and sea ice: (a) top view; (b) side view. Numbers in the figure represents different ice attack angles.

3. Results and Discussion

3.1. Sea Ice Failure Mode

The factors influencing the variation in sea ice failure modes include the loading rate, ice strength, ice plate elastic modulus, ice thickness, structural friction coefficient, structural shape, and structural dynamic characteristics [36]. The ice loads generated via the interaction between sea ice and offshore structures depend on the failure mode of the sea ice, which, in turn, is influenced by factors such as the sea ice velocity and the width of the structure [37]. When sea ice interacts with vertical structures, crushing failure is the main failure mode, and it simultaneously produces the most significant ice load impact. The structures of guide frames are generally smooth cylindrical pile legs. The focus of this research is to determine whether sea ice still undergoes crushing failure after attaching cable pipes to pile legs.

In this section, the sea ice failure modes interacting with such complex structures are analyzed using numerical simulation methods. The analysis encompasses various ice thicknesses, velocities, and attack angles. The entire interaction process is documented, and the changes in the sea ice failure mode following the addition of cable pipes are compared. In the images, it can be observed that sea ice is crushed into a powdered state after interacting with structures. The crushed sea ice continues to interact with the structure, primarily undergoing two forms of failure, as shown in Figure 7. Figure 7a shows that, during the movement of sea ice, the partial adhesion phenomenon may occur on the ice sheet. However, this phenomenon mostly arises during the initial collision between the sea ice and the structure, and it is primarily due to the boundary constraints on ice particles in discrete element method software. Therefore, it is not considered sea ice buckling failure at this time. Figure 7b represents the occurrence of sea ice crushing failure. In the recorded results, the influence of adhesion phenomena is excluded, and the probability of crushing failure is mainly documented.

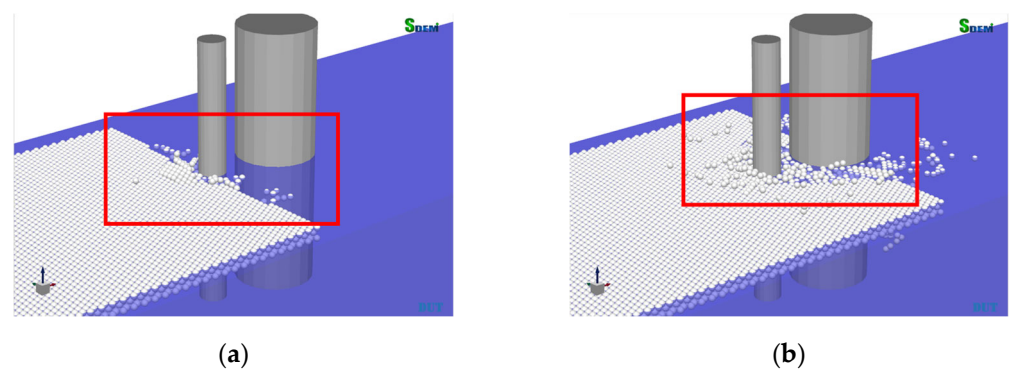


Figure 7. Sea ice failure modes: (a) partial adhesion phenomena; (b) crushing failure.

Table 2 presents the probability of sea ice crushing failure under different ice velocities and ice attack angles when the ice thickness is 0.3 m. The data in Table 2 are also presented in Figures 8 and 9, analyzing the variation in the probability of sea ice crushing failure with ice thickness and ice attack angle.

Table 2. Probability of sea ice crushing failure under different ice velocities and ice attack angles (ice thickness = 0.3 m).

Ice Velocity/m/s	Crushing Failure Probability/%					
	Smooth Cylinder	Ice Attack Angle/°				
		0	30	45	60	90
0.01	95.76	96.88	92.50	95.76	94.44	96.67
0.02	98.31	100.00	95.08	91.30	95.00	96.72
0.03	95.00	92.16	92.31	92.86	95.83	94.12
0.04	94.00	96.08	92.16	96.08	96.08	100.00
0.05	97.56	92.68	96.00	94.12	96.15	92.50
0.06	100.00	95.00	92.68	95.12	96.67	97.56
0.07	97.56	96.08	95.45	93.55	92.11	98.04
0.08	93.75	94.00	92.00	92.00	94.12	92.16
0.09	93.75	95.12	92.68	92.68	94.74	97.37
0.1	100.00	96.77	90.48	91.67	90.48	96.15

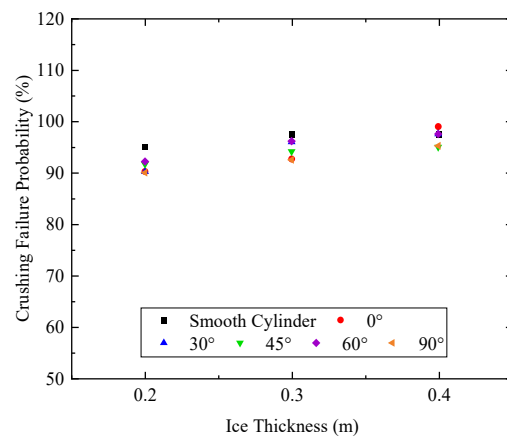


Figure 8. Probability of crushing failure of sea ice under constant ice thickness, constant ice velocity, and different ice attack angles.

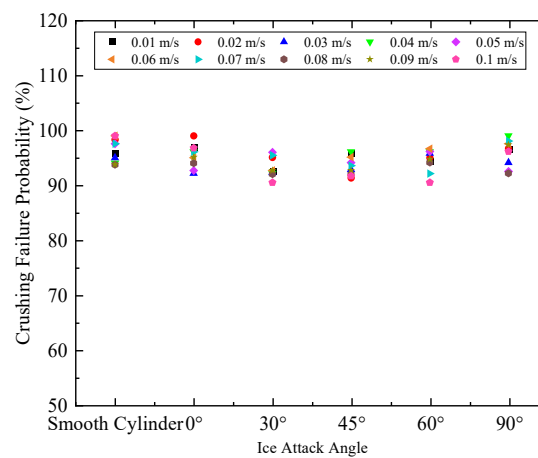


Figure 9. Probability of crushing failure of sea ice under constant ice thickness, constant ice attack angle, and different ice velocities.

According to the results in Figure 8, when the ice thickness and velocity remain constant but the ice attack angle varies, compared to the smooth cylindrical pile leg, the sea ice still primarily experiences crushing failure with an additional cable pipe. Variation in the ice attack angle does not significantly alter the sea ice mode.

As depicted in Figure 9, when the ice thickness and ice attack angle remain constant but the ice velocity varies, the sea ice predominantly undergoes crushing failure, with no substantial alteration in the ice failure mode observed with changes in the ice velocity.

Table 3 presents the probability of sea ice crushing failure under different ice thicknesses and ice attack angles when the ice velocity is 0.05 m/s. The data in Table 3 are also presented in Figure 10, analyzing the change in the probability of sea ice crushing failure with the ice thickness.

Table 3. Probability of sea ice crushing failure under different ice thicknesses and ice attack angles (ice velocity = 0.05 m/s).

Ice Thickness/m	Crushing Failure Probability/%					
	Smooth Cylinder	Ice Attack Angle/°				
		0	30	45	60	90
0.2	95.12	90.24	90.20	91.67	92.16	90.00
0.3	97.56	92.68	96.00	94.12	96.15	92.50
0.4	97.56	100.00	97.56	95.00	97.56	95.24

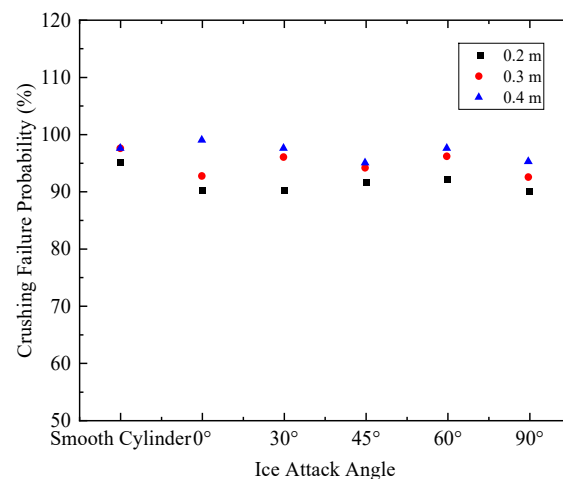


Figure 10. Probability of crushing failure of sea ice under constant ice velocity, constant ice attack angle, and different ice thicknesses.

According to the findings in Figure 10, when the ice velocity and ice attack angle remain constant but the ice thickness varies, the sea ice continues to experience predominantly crushing failure, and the trend of crushing failure becomes more pronounced with increasing ice thickness.

In conclusion, compared to the smooth cylindrical pile leg, the interaction between offshore substation structures and sea ice after the addition of cable pipes does not change the sea ice failure mode significantly, and sea ice still primarily undergoes crushing failure. This is because the size of the cable pipes is small relative to that of the pile legs, resulting in a narrower area of ice failure. The broken ice is subjected to greater restraining forces from the surrounding ice. Consequently, the ice is unlikely to fracture further from the initial breakage point in most cases. Therefore, the interaction between the ice and the pile legs primarily results in crushing failure.

3.2. Ice Force Amplitude

In previous research, the two different analysis methods described below are generally selected to calculate the ice force amplitude on offshore substation structures with additional cable pipes. Firstly, the ice force amplitudes on the cable pipe and the leg of the offshore substation structure are calculated, and the ice force amplitudes of the two are algebraically summed as the estimation of the total ice force amplitude (hereinafter referred to as the “Sum Method”). Secondly, a comprehensive method is adopted; that is, the cable pipe and the leg of the offshore substation structure are regarded as a unified whole, and the ice force amplitude on the whole is estimated by calculating its equivalent diameter (hereinafter referred to as the “Dia Method”).

This section employs numerical simulation methods to analyze the ice force amplitude when sea ice interacts with complex structures under different ice thicknesses, velocities, and attack angles. By selecting the maximum values within the time history for a data analysis and comparing them with the ice force amplitude on a smooth cylindrical pile leg, the variations in structural ice force amplitude with the addition of cable pipes are investigated. Table 4 presents the statistical results of the ice force amplitude on the structure under different ice velocities and ice attack angles when the ice thickness is 0.3 m. The data in Table 4 are also presented in Figures 11 and 12, analyzing the variation in ice force amplitude with the ice attack angle and ice velocity.

Table 4. Ice force amplitude under different ice velocities and ice attack angles (ice thickness = 0.3 m).

Ice Velocity/m/s	Ice Force Amplitude/kN					
	Smooth Cylinder	Ice Attack Angle/°				
		0	30	45	60	90
0.01	354.36	441.23	318.47	308.03	303.62	293.12
0.02	429.21	484.79	324.46	312.47	311.42	301.43
0.03	306.59	368.65	290.21	277.11	275.78	270.21
0.04	401.86	458.38	362.95	357.11	352.20	335.86
0.05	344.32	373.05	322.62	312.18	305.25	275.52
0.06	419.00	471.31	361.53	351.45	343.59	341.13
0.07	378.87	415.55	329.42	291.20	289.14	282.46
0.08	305.83	373.42	278.99	272.93	269.34	257.32
0.09	345.33	409.57	299.76	291.65	287.93	282.23
0.1	297.07	371.16	278.20	271.25	269.64	268.58

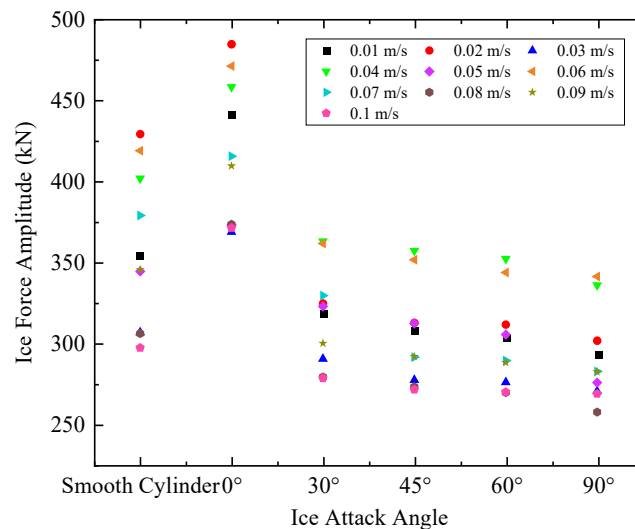


Figure 11. Ice force amplitude under constant ice thickness, constant ice velocity, and different ice attack angles.

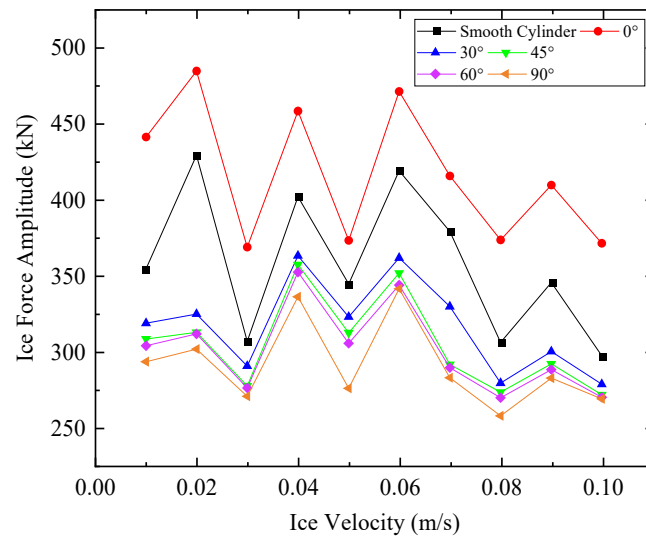


Figure 12. Ice force amplitude under constant ice thickness, constant ice attack angle, and different ice velocities.

According to the results in Figure 11, under the same ice velocity and thickness conditions with varying ice attack angles, the addition of cable pipes leads to an ice–structure interaction where, except for at a 0° ice attack angle, the sea ice collides with the cable pipes before interacting with the structural pile legs, followed by an interaction with the broken ice. As the diameter of the cable pipes is smaller than that of the pile legs, the contact area with the sea ice decreases, resulting in a reduction in the ice force amplitude, with the smallest value occurring at a 90° ice attack angle. However, at a 0° ice attack angle, after the interaction between the sea ice and the structure, the interaction width increases compared to that of the smooth cylindrical pile legs, resulting in the largest value.

Meanwhile, when the ice thickness is 0.3 m, compared to the ice force amplitude experienced by the smooth cylindrical pile legs, the following proportional changes are observed. At a 0° ice attack angle, the increase in the ice force amplitude ranges between 8% and 25%; at a 30° ice attack angle, the decrease is roughly distributed between 6% and 14%; at a 45° ice attack angle, the decrease is roughly distributed between 8% and 16%; at a 60° ice attack angle, the decrease is roughly distributed between 9% and 18%; and at a 90° ice attack angle, the decrease is roughly distributed between 10% and 20%.

According to the results in Figure 12, under the same ice thickness and ice attack angle conditions, varying ice velocities lead to the following observations. When the ice velocity is within the range of 0.01 m/s to 0.06 m/s, the ice force amplitude varies with no clear pattern, mainly influenced by structural vibration and sea ice ductile–brittle failure, resulting in random fluctuations in the ice force amplitude. When the ice velocity is between 0.06 m/s and 0.1 m/s, the sea ice undergoes brittle failure, with a relatively small variation in the ice force amplitude, showing a decreasing trend.

Table 5 presents the statistical results of the ice force amplitude on the structure under different ice thicknesses and ice attack angles when the ice velocity is 0.05 m/s. The data in Table 5 are presented in Figure 13, analyzing the variation in ice force amplitude with ice thickness.

According to the results in Figure 13, it can be observed that, under the same ice velocity and ice attack angle conditions, with an increase in ice thickness, the contact area between the sea ice and the structure increases, leading to an upward trend in the ice force amplitude. When the ice velocity is 0.05 m/s, compared to the ice force amplitude experienced by the smooth cylindrical pile legs, the proportional changes under the different ice attack angles are as follows. The ice force amplitude exhibits an increase of 8–9.5% at an ice attack angle of 0°; a decrease of 6–8% at 30°; a decrease of 8–10% at 45°; a decrease of

10–12% at 60°; and a decrease of 19–20% at 90°. Additionally, there is an increase of 58–60% when using the Sum Method and an increase of 17–18% when using the Dia Method.

Table 5. Ice force amplitude under different ice thicknesses and ice attack angles (ice velocity = 0.05 m/s).

Ice Attack Angle/°	Ice Force Amplitude/kN		
	Ice Thickness/m		
	0.2	0.3	0.4
Smooth Cylinder	298.46	344.32	397.61
0°	325.70	373.05	431.12
30°	275.99	322.62	371.01
45°	272.25	312.18	366.11
60°	264.41	305.25	355.23
90°	241.68	275.52	319.17
Dia Method	472.59	546.63	640.05
Sum Method	351.44	404.37	466.49

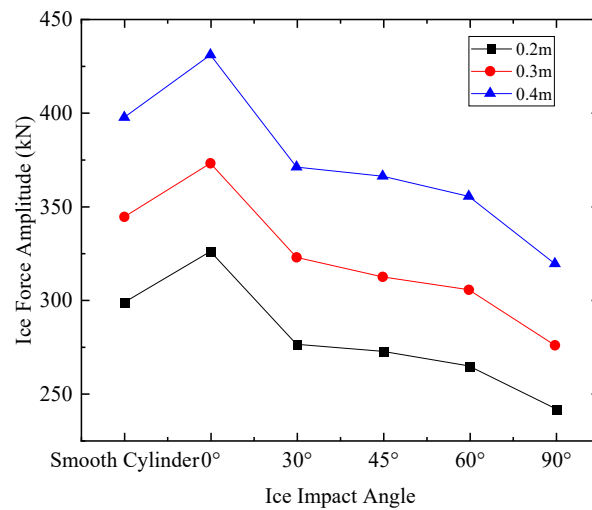


Figure 13. Ice force amplitude under constant ice velocity, constant ice attack angle, and different ice thicknesses.

3.3. Ice Force Variation Coefficient

According to Formula (6), the ratio γ_n of the ice force amplitude obtained under different ice attack angles or calculation methods to the ice force amplitude of the smooth cylindrical pile legs is calculated, defining it as the ice force variation coefficient. The data in Tables 4 and 5 are combined to calculate coefficient γ_n , and they are plotted in Figure 14. After excluding randomness, the mean is computed, and, finally, the calculation parameters of the ice load model for such structures are defined, as shown in Table 6.

$$\gamma_n = \frac{F_n}{F_z} \tag{6}$$

Table 6. Calculation parameters of ice load model of offshore substation structure with cable pipe.

Different Ice Attack Angles or Calculation Methods	γ_n	Different Ice Attack Angles or Calculation Methods	γ_n
0°	1.10	90°	0.78
30°	0.90	Sum Method	1.59
45°	0.87	Dia Method	1.18
60°	0.85		

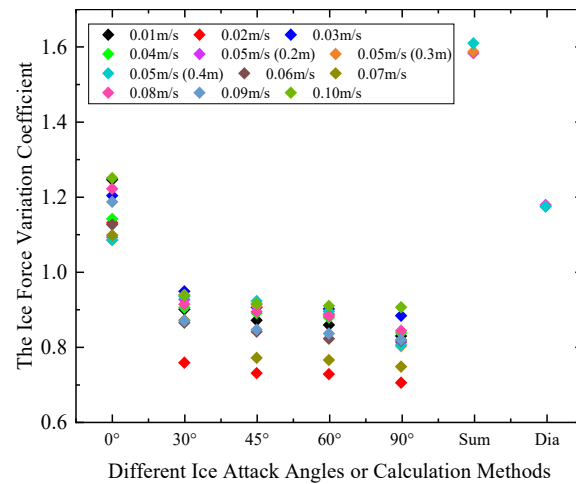


Figure 14. The ice force variation coefficient under different ice attack angles/calculation methods.

4. Conclusions

In this study, numerical modeling techniques are employed to simulate the interaction between offshore substation structures and sea ice. Compared to jacket platforms, offshore substation structures have additional structure cable pipes on their piles. The research on ice loads for such complex structures includes variations in the sea ice failure mode and ice force amplitude with the cable pipes.

In terms of the sea ice failure mode, when sea ice interacts with smooth cylindrical pile legs, it mainly undergoes crushing failure. Similarly, when interacting with additional cable pipe structures, alterations in the ice thickness, velocity, and attack angle still result primarily in crushing failure. Moreover, as the ice thickness increases, the trend towards crushing failure becomes more pronounced.

In terms of the ice force amplitude, the addition of cable pipes to offshore substation structures affects the ice force amplitude. The ice force amplitude is minimum when the ice attack angle is 90° and maximum when it is 0°. The ice force amplitude varies unpredictably with ice velocity and exhibits randomness. When the ice velocity is between 0.06 m/s and 0.1 m/s, sea ice undergoes brittle crushing failure; furthermore, the variation in ice force amplitude is minor, and it shows a decreasing trend. The ice force amplitude increases with ice thickness.

Based on ice force variation coefficient γ , the ice force amplitudes under different ice attack angles/calculation methods are determined. Compared to traditional methods such as the Sum Method and Dia Method, the ice load calculation method proposed in this paper can more reasonably assess the ice loads on additional cable pipe pile legs, thereby enhancing the economic efficiency of structural design. The research presented here relies primarily on numerical simulation methods, and validation and further analysis of such issues can be achieved through model tests or field monitoring. Additionally, research is being conducted on the pattern changes in ice-induced steady-state vibrations caused by additional cable pipes.

Author Contributions: B.Z.: Formal analysis, visualization and writing—original draft; R.D.: Resources, software, data curation and writing—original draft; W.L.: Methodology, investigation and writing—review and editing; Y.Z.: Methodology, validation, and writing—review and editing; G.W.: Software, data curation and writing—review and editing; D.Z.: Conceptualization, writing—review and editing, and supervision. All authors have read and agreed to the published version of the manuscript.

Funding: This work was funded by the National Natural Science Foundation of China (Grant No.52071055), and the Fundamental Research Funds for the Central Universities (Grant No. DUT22QN237), and the National Key Research and Development Program of China (Grant No. 2023YFC2809104), and the Liaoning Provincial Natural Science Foundation Joint Fund (Grant No. DUT24BS031).

Institutional Review Board Statement: Not applicable.

Informed Consent Statement: Not applicable.

Data Availability Statement: The original contributions presented in the study are included in the article, further inquiries can be directed to the corresponding author.

Conflicts of Interest: B.Z., W.L. and Y.Z. were employed by “PowerChina Huadong Engineering Corporation Limited”. The remaining authors declare that the research was conducted in the absence of any commercial or financial relationships that could be construed as a potential conflict of interest.

References

1. Wang, A.L.; Tang, M.N.; Zhao, Q.; Liu, Y.; Li, B.H.; Shi, Y.Y.; Sui, J.P. Analysis of sea ice parameters for the design of an offshore wind farm in the Bohai Sea. *Ocean Eng.* **2021**, *239*, 109902. [[CrossRef](#)]
2. Haselbozchaloe, D.; Correia, J.; Mendes, P.; Jesus, A.D.; Berto, F. A review of fatigue damage assessment in offshore wind turbine support structure. *Int. J. Fatigue* **2022**, *164*, 107145. [[CrossRef](#)]
3. Wang, G.J.; Yue, Q.J.; Zhang, D.Y.; Fu, Y.H.; Peng, X.; Dong, R. Distribution analysis of local ice pressures in the indentation test at various velocities. *J. Mar. Sci. Eng.* **2022**, *10*, 433. [[CrossRef](#)]
4. Timco, G.W.; Johnston, M. Ice loads on the caisson structures in the Canadian Beaufort Sea. *Cold Reg. Sci. Technol.* **2004**, *38*, 185–209. [[CrossRef](#)]
5. Kärnä, T.; Kamesaki, K.; Tsukuda, H. A numerical model for dynamic ice-structure interaction. *Comput. Struct.* **1999**, *72*, 645–658. [[CrossRef](#)]
6. Kärnä, T.; Jochmann, P. Field observations on ice failure modes. In Proceedings of the 17th International Conference on Port and Ocean Engineering under Arctic Conditions, Trondheim, Norway, 16–19 June 2003.
7. Hendrikse, H.; Metrikine, A. Ice-induced vibrations and ice buckling. *Cold Reg. Sci. Technol.* **2016**, *131*, 129–141. [[CrossRef](#)]
8. Yue, Q.J.; Guo, F.W.; Kärnä, T. Dynamic ice forces of slender vertical structures due to ice crushing. *Cold Reg. Sci. Technol.* **2009**, *56*, 77–83. [[CrossRef](#)]
9. Sanderson, T. *Ice Mechanics and Risks to Offshore Structures*; Kluwer Academic Publishers: Norwell, MA, USA, 1988.
10. Ji, S.Y.; Di, S.C.; Liu, S.W. Analysis of ice load on conical structure with discrete element method. *Eng. Comput.* **2015**, *32*, 1121–1134. [[CrossRef](#)]
11. Long, X.; Liu, L.; Ji, S.Y. Discrete element analysis of ice-induced vibrations of offshore wind turbines in level ice. *J. Mar. Sci. Eng.* **2023**, *11*, 2153. [[CrossRef](#)]
12. Izumiyama, K.; Kitagawa, H.; Koyama, K.; Uto, S. On the interaction between a conical structure and ice sheet. In Proceedings of the 11th International Conference on Port and Ocean Engineering under Arctic Conditions, St. John’s, NL, Canada, 24–28 September 1991; Volume 1, pp. 155–166.
13. Li, F.; Yue, Q.J. Failure mode effect on conical structure dynamic ice forces. In Proceedings of the 19th International Conference on Port and Ocean Engineering under Arctic Conditions, Dalian, China, 27–30 June 2007; pp. 113–121.
14. Paavilainen, J.; Tuhkuri, J. Ice loads on sloping structures: Influence of parameters in virtual experiments. In Proceedings of the 21st IAHR International Symposium on Ice, Dalian, China, 11–15 June 2012; pp. 842–852.
15. Qu, Y.; Yue, Q.J.; Bi, X.J.; Kärnä, T. A random ice force model for narrow conical structures. *Cold Reg. Sci. Technol.* **2006**, *45*, 148–157.
16. Ranta, J.; Polojarvi, A.; Tuhkuri, J. Limit mechanisms for ice loads on inclined structures: Buckling. *Cold Reg. Sci. Technol.* **2018**, *147*, 34–44. [[CrossRef](#)]
17. Ranta, J.; Polojarvi, A.; Tuhkuri, J. Ice loads on inclined marine structures-Virtual experiments on ice failure process evolution. *Mar. Struct.* **2018**, *57*, 72–86. [[CrossRef](#)]
18. Ranta, J.; Polojarvi, A.; Tuhkuri, J. The statistical analysis of peak ice loads in a simulated ice-structure interaction process. *Cold Reg. Sci. Technol.* **2017**, *13*, 46–55. [[CrossRef](#)]
19. Di, S.C.; Xue, Y.Z.; Wang, Q.; Bai, X.L. Discrete element simulation of ice loads on narrow conical structures. *Ocean Eng.* **2017**, *146*, 282–297. [[CrossRef](#)]
20. Jou, O.; Celigueta, M.A.; Latorre, S.; Arrufat, F.; Onate, E. A bonded discrete element method for modeling ship-ice interactions in broken and unbroken sea ice fields. *Comput. Part. Mec.* **2019**, *6*, 739–765. [[CrossRef](#)]
21. Chen, Y.H.; Liu, H.Y. Overview of the development of offshore wind power generation in China. *Sustain. Energy Technol. Assess.* **2022**, *53*, 102766. [[CrossRef](#)]
22. Zhang, D.Y.; Qu, Y.; Yue, Q.J.; Xu, N. Ice-Resistant performance analysis of jackup structures. *J. Cold Reg. Eng.* **2018**, *32*, 04017022. [[CrossRef](#)]
23. Liu, H.J.; Tian, Y.F. Model test of ice load on high pile cap foundation of offshore wind power. *China Offshore Platf.* **2020**, *35*, 54–59.
24. *Regulations for Offshore Ice Condition & Application in China Sea: Q/HSn 3000-2002*; China National Offshore Oil Corporation: Beijing, China, 2002.
25. Chen, Z.A.; Huang, Y.T.; Zhang, D.Y. Machine learning assisted in forecasting the ice-induced vibration for jacket platforms. *Appl. Ocean Res.* **2023**, *141*, 103778. [[CrossRef](#)]

26. Shen, H.H.; Ackley, S.F.; Yong, Y. Limiting diameter of pancake ice. *J. Geophys. Res.-Oceans* **2004**, *109*, 1–13. [[CrossRef](#)]
27. Dempsey, J.P. Research trends in ice mechanics. *Int. J. Solids Struct.* **2000**, *37*, 131–153. [[CrossRef](#)]
28. Hopkins, M.A. Four stages of pressure ridging. *J. Geophys. Res.-Oceans* **1998**, *103*, 21883–21891. [[CrossRef](#)]
29. Liu, M.H.; Wang, Q.; Lu, W. Peridynamic simulation of brittle-ice crushed by a vertical structure. *Int. J. Nav. Arch. Ocean Eng.* **2017**, *9*, 209–218. [[CrossRef](#)]
30. Long, X.; Liu, S.W.; Ji, S.Y. Discrete element modelling of relationship between ice breaking length and ice load on conical structure. *Ocean Eng.* **2020**, *201*, 107152. [[CrossRef](#)]
31. Ji, S.Y.; Li, Z.L.; Li, C.H.; Shang, J. Discrete element modeling of ice loads on ship hulls in broken ice fields. *Acta Oceanol. Sin.* **2013**, *32*, 50–58. [[CrossRef](#)]
32. Ji, S.Y. Discrete Element Modeling of Ice loads on ship and offshore structures. In Proceedings of the 7th International Conference on Discrete Element Methods, Dalian, China, 1–4 August 2016; pp. 45–54.
33. Potyondy, D.O.; Cundall, P.A. A bonded-particle model for rock. *Int. J. Rock Mech. Min.* **2004**, *41*, 1329–1364. [[CrossRef](#)]
34. Wilchinsky, A.V.; Feltham, D.L.; Hopkins, M.A. Modelling the reorientation of sea-ice faults as the wind changes direction. *Ann. Glaciol.* **2011**, *52*, 83–90. [[CrossRef](#)]
35. Jang, H.K.; Kim, M. Dynamic ice force estimation on a conical structure by discrete element method. *Int. J. Nav. Arch. Ocean Eng.* **2021**, *13*, 136–146. [[CrossRef](#)]
36. Timco, G.W.; Sudom, D. Revisiting the Sanderson pressure–area curve: Defining parameters that influence ice pressure. *Cold Reg. Sci. Technol.* **2013**, *95*, 53–66. [[CrossRef](#)]
37. Sodhi, D.S.; Haehnel, R.B. Crushing ice forces on structures. *J. Cold Reg. Eng.* **2003**, *17*, 135–184. [[CrossRef](#)]

Disclaimer/Publisher’s Note: The statements, opinions and data contained in all publications are solely those of the individual author(s) and contributor(s) and not of MDPI and/or the editor(s). MDPI and/or the editor(s) disclaim responsibility for any injury to people or property resulting from any ideas, methods, instructions or products referred to in the content.